Macromolecules

ARTICLE

pubs.acs.org/Macromolecules

Structure and Conformations of Polymer/SWCNT Nanocomposites

Argyrios Karatrantos,[†] Russell J. Composto,[‡] Karen I. Winey,[‡] and Nigel Clarke*[,†]

[†]Department of Physics and Astronomy, University of Sheffield, Sheffield S3 7RH, United Kingdom

[‡]Department of Materials Science and Engineering, University of Pennsylvania, Philadelphia, Pennsylvania 19104, United States

ABSTRACT: We investigate the static properties of monodisperse polymer/single wall carbon nanotube (SWCNT) nanocomposites in comparison to polymer melts by molecular dynamics simulations. The SWCNT has a large aspect ratio and radius smaller than the polymer radius of gyration. We find that although the local chain structure is significantly affected, the overall configuration, as characterized by the radius of gyration, is not perturbed either by the interaction strength between the polymer and the SWCNT or by variations in the SWCNT radius.

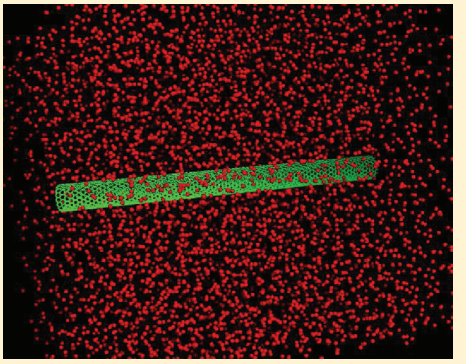

I. INTRODUCTION

Polymer nanocomposites, that is, nanoparticles (spheres, cylinders, plates) dispersed in an entangled matrix, have attracted substantial academic and industrial interest since the early 1990s.[1−7] It is well recognized that the addition of nanoparticles to a polymer can result in materials that have significantly improved properties, such as flame retardation, electrical conductivity, thermal conductivity, impact strength, and viscosity. The interest in polymer−carbon composites[3,4,7−16] has rapidly increased since carbon nanotubes became widely available in the late 1990s. There have been many studies in the area of polymer/SWCNT nanocomposites that have investigated dynamic, electrical, thermal, and rheological properties;[3,4,6−14,17] however, to the best of our knowledge, no study has addressed static properties in a polymer/SWCNT nanocomposite system. In this study we focus on a dilute SWCNT nanocomposite system, where recently it was found that the polymer diffusion is suppresed when the polymer radius of gyration is larger than the radius of the nanotube.[11,12] Because of the large aspect ratio of the SWCNT, the percolation threshold appears at volume fraction[10−12] of 0.4%. We explore the polymer/SWCNT interface and focus on simple but unresolved questions in the area of polymer/SWCNT nanocomposites: (i) What is the effect of SWCNT on polymer chain conformation? (ii) How is interchain packing perturbed by monomer−SWCNT interactions and SWCNT radius? In this paper, we provide a systematic simulation study which sheds light on how the interaction between polymer chains and SWCNT and polymer confinement between SWCNTs affect the structure and conformation of different molecular weight polymer chains in the vicinity of the SWCNT, for nanocomposite systems where polymer radius of gyration is larger than the radius of the SWCNT.[11,12]

Few experimental studies have been undertaken on the structure and conformation of polymers loaded with spherical nanoparticles.[5,18−24] There is controversy as to whether the addition of nanoparticles to a polymer melt causes perturbed behavior of polymers near the spherical nanoparticles. In particular, neutron scattering of a polystyrene (PS) chains/(PS) nanoparticles nanocomposite[19,22] showed a polymer chain expansion for polymer chains with radius of gyration larger than the nanoparticle radius, which is contrary to other recent studies of PS/silica[21,23] and poly(ethylene−propylene)/silica[24] nanocomposites that showed the polymer chains to be unperturbed. Moreover, in a former study of a poly(dimethylsiloxane)/polysilicate nanocomposite,[18] an increase of polymer chain dimensions is observed: in agreement with the observations of Mackay.[19,22]

Over the past two decades, many efforts have been made to predict and investigate through theoretical,[25−31] coarse-grained,[32−59] and atomistic simulation[60] the structure and conformation of polymer nanoparticle solutions. Almost all of these studies investigate the effect of spherical nanoparticles on the polymer radius of gyration and structure of polymer chains. From a theoretical point of view, mean-field[25−27,30] and self-consistent-field[28,29] theories predict that monomers are depleted around the spherical nanoparticles, where the density of polymers is reduced compared to its bulk value. Recently, by using the self-consistent polymer reference interaction site model (SC/PRISM),[31] it was observed that spherical nanoparticles, smaller than the polymer chains and attracted to them, perturb the polymer chain dimensions. The nanoparticles cause an increase in the radius of gyration with an increase in the nanoparticle volume fractions in accordance to the (PS) nanoparticle system,[19,22] although there are significant differences between the theoretical model system

Received: June 16, 2011
Revised: November 1, 2011
Published: November 22, 2011

and the experimental one. Some of the expansion is due to the effects of the excluded volume created by the nanoparticles; the nanoparticles act as good solvents to swell the polymers. From a simulation point of view, the applicability of earlier studies,[32−34] for high and moderate filler systems, was unclear[38] due to the assumption of noninteracting chains and also due to the fact that polymer chains are too short to be directly compared to chains found in many real systems.[38] In further studies of polymer structure in the vicinity of the spherical surface, the monomer density was found to be lower at the surface than in the bulk.[40,46,58] In contrast, when the polymer chains are attracted to spherical nanoparticles,[36−39,41−45,48−52,54−57,59,60] the monomer density is higher in the vicinity of the spherical nanoparticles than in the bulk. Nevertheless, there is controversy as to whether the addition of attractive nanoparticles to a polymer melt causes polymer chains to either expand,[36,39,51,55,59,60] remain unaltered,[41,48,50] or reduce their dimensions[37,38,44] compared to their size in the bulk. While most of the simulation studies were performed for nanocomposites systems where the nanoparticle's size is similar to the polymer size,[36,39,48,54,55,60] it is well recognized[18−21,24,42,53,61,62] that in the case of polymer−nanoparticles mixtures their final structures are strongly influenced by the characteristics of nanoparticles (e.g., size, shape, aspect ratio, type of nanoparticle surface, surface area, volume fraction of nanoparticles) and the polymer (e.g., molecular weight, structure, nature of the interactions between the nanoparticle and the polymer matrix).

Furthermore, the interface between oligomers and single wall carbon nanotubes (SWCNTs) has been the subject of several simulation studies in recent years.[53,63−69] In particular, the intermolecular interaction between different kinds of oligomers (such as flexible backbones (poly(methyl methacrylate)), flexible backbones with bulky groups (polystyrene), and high rigid backbones (polythiophene)) and SWCNT[63,65,66] and also the conformation of oligomers[63,66] have been studied extensively by conducting very short atomistic simulations in vacuo. These studies showed on one hand that there are attractive interactions between the oligomers and SWCNT[63,65,66] which increase with greater radius of SWCNT, tending toward the limit of a graphene surface.[63,66] On the other hand, the structure of the oligomers is not changed by the interaction with the SWCNT for the cases of flexible backbones with bulky groups[63] and highly rigid backbones;[66] thus, these types of oligomers remain unperturbed by the SWCNT interaction. It is worth noting that there have been recent studies, by coarse-grained simulations, of the role of hydrophobic interactions on the wrapping mechanism and physical adsorption of DNA in aqueous environment[70] or entangled polymers[68,69] on carbon nanotubes. Moreover, by using atomistic simulations, the wrapping mechanism has been investigated further for different kinds of molecules (such as DNA, flexible backbone, and rigid backbones polymers) around the SWCNT to ascertain how the wrapping is affected, not only by the chemical composition or structure of the molecules[66,67,71,72] but also by the lattice structure of the SWCNT, radius of the SWCNT, and the temperature.[64] Although the analysis of an atomic-level simulation provides a useful insight into the interaction of oligomers with an individual SWCNT, for a polymer/SWCNT nanocomposite system it is important to relate the polymer−SWCNT interaction with the monomer−monomer interaction and understand how both affect the static properties of polymer chains.

The rest of this paper is organized as follows. In section II, we present the general features of the simulation methodology and simulation details that were used to investigate the static properties of polymer melts and polymer nanocomposites. Subsequently in the same section, the theoretical background is given for the static properties that are usually studied in polymer melts and polymer nanocomposites. In section III.A, we discuss the structure of both unentangled and entangled polymer chains, using a coarse-grained model and analyze its conformation through the calculation of the end-to-end distance and radius of gyration. In section III.B, we consider a polymer/SWCNT nanocomposite system where a long SWCNT is inserted in the simulation cell. The structure and conformation of all the polymer chains are explored and compared with those of the polymer melt at different interaction strengths and various radii of SWCNT. In addition, we focus on the static properties of the polymer chains that are in contact with the SWCNT to allow comparison with recently studied experimental systems. Furthermore, we have performed simulations with two SWCNTs present in the simulation cell in order to investigate confinement effects on the polymer chain structure. Finally, in section IV, conclusions of the study are given.

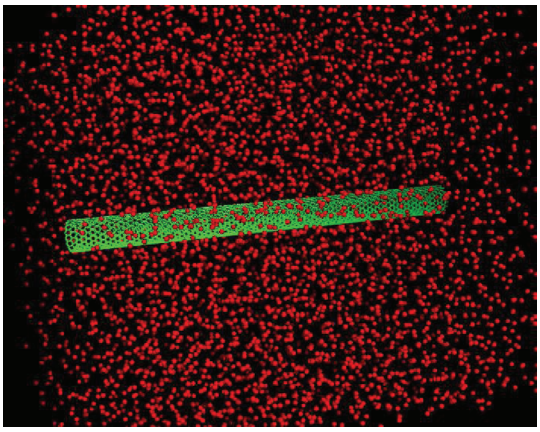

Figure 1. Model of the nanocomposite system (SWCNT in polymer matrix) along the *z*-axis. For clarity, the connectivity of the beads is not shown.

II. SIMULATION METHODOLOGY AND STATIC PROPERTIES

We performed molecular dynamics simulations of monodisperse polymer melts and monodisperse polymer/SWCNT nanocomposite systems. The polymer melt is simulated by using a coarse-grained polymer model.[73,74] In a well-dispersed PS/SWCNT nanocomposite the radius of the nanotube is of the order of the Kuhn length of PS. Consequently, in the nanocomposite system simulations, an atomistic model was used for the SWCNT. Thus, we include the influence not only of the geometric characteristics but also the SWCNT structure surface on the polymer properties. Polymer chains are composed of bead−spring chains of Lennard-Jones (LJ) monomers m, of diameter $\sigma_m = 1$ and mass $m_m = 1$. Three different SWCNTs ((12,0), (17,0), (22,0) of radius $r_{SWCNT} = 0.46\sigma_m$, $0.66\sigma_m$, $0.85\sigma_m$, respectively) are considered and span the simulation cell with their atoms held fixed in a centered position in the simulation cell along the *z*-axis. A molecular model of the nanocomposite system is shown in Figure 1. In the case of confined systems, two SWCNTs ((17,0)) are inserted in the simulation cell. The SWCNTs are fixed in space and separated with a distance of R_g.

Nonbonded monomer−monomer as well as monomer (m)−carbon (c) interact via a truncated and shifted Lennard-Jones (LJ) potential,[75,76] with a cutoff radius $r_c = 2.3\sigma_m$, given by[77−80]

$$U_{LJ}(r_{ij}) = \begin{cases} 4\varepsilon\left[\left(\frac{\sigma_{ij}}{r_{ij}}\right)^{12} - \left(\frac{\sigma_{ij}}{r_{ij}}\right)^{6} - C(r)\right] & \text{for } r < r_c \\ 0 & \text{for } r \geq r_c \end{cases} \quad (1)$$

where $C(r)$[77−80] is a third degree polynomial which is added so that the potential vanishes continuously at $r = r_c$, ε is a characteristic interaction energy (interaction strength) between particles, and r_{ij} is the distance between particles i and j. The interaction energy between monomers is $\varepsilon_{mm} = kT = 1$ (where k is Boltzmann's constant and T is temperature). The distance between the carbon atoms in the SWCNT is 0.1415. Thus, for the monomer carbon interaction, we use a geometric mean combination rule: $\sigma_{mc} = (\sigma_c\sigma_m)^{1/2} = (0.141 \cdot 1)^{1/2} = 0.3755$. The interaction energy between monomer and carbon, ε_{mc}, varies between 0 and $5kT$. For the simulations where the polymers have no interaction with the nanotube surface, only the repulsive term of eq 1 is retained, and in order to have a very slight repulsion, $\varepsilon_{mc} = 5 \times 10^{-4}kT$.

For nearest-neighbor monomers along the chain the LJ interaction is not included. Technically, these monomers are connected to each other by a harmonic bond potential,[73,74] given by

$$U_{bond}(r) = \frac{K}{2}(r - r_0)^2 \quad (2)$$

with an equilibrium bond length $r_0 = 0.967\sigma_m$ and a spring constant $K = 1111$.[73,74] The value of K is large enough to prevent the chains from cutting through each other in the simulation, which allows the formation of entanglements. It is worth noting that the entanglement length of this polymer coarse-grained model, for $N = 128$, is $N_e = 36$ as calculated by the Z1 algorithm[81,82] based on an analysis of 15 configurations.

A. Simulation Details. In this study, *NVT* molecular dynamics simulations were performed using the GROMACS package[77−80] at a melt density $\rho^* = (N_m/V)\sigma_m^3 = 0.85$ (where N_m is the total number of monomers in the system and V is the volume of the polymer melt). In any simulation of the nanocomposite system, the monomer density was retained to its melt value, and one SWCNT was inserted in the simulation cell, so that simulations were performed at filler volume fraction of 0.4% in accordance with a recently studied PS/SWCNT nanocomposite.[11,12] In the case of confined systems, the filler volume fraction is 0.8%. The length of the simulation cell was always larger than the end-to-end distance of the polymer chains. In order to set the temperature at $T^* = kT/\varepsilon = 1$, the Nose−Hoover[83,84] thermostat was used with an oscillation relaxation constant $\tau_T = 2.0\tau$.

The equations of motion were integrated using the leapfrog algorithm[85] with a time step equal to 0.005τ, where $\tau = (m\sigma_m^2/kT)^{1/2}$ is the Lennard-Jones time. The duration of the simulation runs were between $30 \times 10^6\tau$ and $50 \times 10^6\tau$ depending on the length of molecules and system (polymer melt or nanocomposite) studied. The time needed for the end-to-end vector autocorrelation for 60-mer polymers to decay to zero is $\sim 10000\tau$. The static properties of the polymer chains were calculated after 20×10^6 steps for the polymer melts and after 30×10^6 steps for the nanocomposite systems. The polymer chains diffuse several R_g distance during the simulation; for example, 60-mer polymers diffuse $7R_g$ in nanocomposite simulations when the attraction from the nanotube surface is kT. The polymers in contact with the nanotube diffuse $3.5R_g$ and R_g distance when the attraction from the nanotube surface is kT and $2.5kT$, respectively.

Table 1. Number of Polymer Chains N_p, Number of Monomers N in a Polymer Chain, Length of the Simulation Cell L, Polymer Radius of Gyration R_g, and End-to-End Distance R_e for Polymer Melt Systems Studied in the Present Simulation[a]

N_p (polymer chains)	N (monomers)	L_{cell}	R_g	R_e
256	10	14.441	1.451 (0.029)	3.582 (0.072)
256	12	15.346	1.605 (0.034)	3.977 (0.083)
256	16	16.891	1.901 (0.021)	4.729 (0.098)
128	20	14.441	2.158 (0.037)	5.393 (0.625)
192	30	18.923	2.751 (0.044)	6.761 (0.044)
64	32	13.406	2.794 (0.067)	7.019 (0.307)
72	40	15.02	3.139 (0.074)	7.888 (0.314)
96	50	17.808	3.557 (0.069)	8.939 (0.34)
96	60	18.923	3.886 (0.084)	9.688 (0.389)
96	64	19.335	4.072 (0.125)	10.24 (0.305)
20	128	14.441	5.688 (0.28)	14.751 (1.61)

[a] The values in parentheses are the error bars. The monomer density is $\rho^* = 0.85$ for all the runs.

Table 2. Type of SWCNT, Total Number of Monomers N_m in the Simulation Cell, Length of the Simulation Cell in the x or y and z Direction ($L_{x,y}$, L_z), Respectively

SWCNT	N_m	$L_{x,y}$	L_z
(12,0)	5760	14.431	32.648
(17,0)	5760	18.96	18.923
(22,0)	11520	24.536	22.598

The details (number of polymer chains N_p, number of monomers N, length of the cubic simulation cell L_{cell}, polymer radius of gyration, R_g, polymer end-to-end distance, R_e) of the polymer melt and nanocomposite simulated systems are given in Tables 1 and 2.

B. Static Properties. In this section of the paper, we will discuss the static properties, and their theoretical background, in terms of how they are usually studied in both polymer melts and nanocomposite systems. In particular, in a polymer melt, polymer chains are supposed to be ideal in the sense that they obey random walk statistics. Thus, the end-to-end distance R_e of a polymer chain is given by[86−88]

$$\langle R_e^2(N)\rangle = \langle(\mathbf{r}_1 - \mathbf{r}_N)^2\rangle = l_k L = l_k^2 N_k \quad (3)$$

where $\mathbf{r}_1$, $\mathbf{r}_N$ are the coordinates of the chain ends, l_k is the Kuhn length, L is the contour length, and N_k are the number of Kuhn steps of the polymer chain. Also, another static property that gives information about the conformation of the polymer chains is the radius of gyration of a molecule, which is defined as the average squared distance between monomers in given conformation and the molecule's center of mass and is given by[86,87]

$$\langle R_g^2(N)\rangle = \frac{1}{N}\left\langle \sum_{i=1}^{N} (\mathbf{r}_i - \mathbf{r}_{cm})^2 \right\rangle \quad (4)$$

where $\mathbf{r}_{cm} = (1/N)\Sigma_{i=1}\mathbf{r}_i$ is the center of mass of the chain. Similarly to eq 3, the radius of gyration follows the following scaling relation:

$$\langle R_g^2(N)\rangle \sim N_k \quad (5)$$

Furthermore, the radius of gyration about an axis j can give us further information about the conformation of the chain around the SWCNT and is given by

$$\langle R_g^2(N)\rangle = \frac{1}{N}\left\langle \sum_{i=1}^{N} (j_i - j_{cm})^2 \right\rangle \quad (6)$$

where $j_i = (x_i, y_i, z_i)$ are the positions of the ith atom and $j_{cm} = (x_{cm}, y_{cm}, z_{cm})$ are the positions of the center of mass.

In addition, another static property that has been largely studied in polymer melts and polymer nanocomposites is the radial distribution function (rdf) or pair correlation function $g(r)$. In general, the $g_{AB}(r)$ between two particles A and B is defined by[75−77]

$$g_{AB}(r) = \frac{V}{4\pi r^2}\sum_{i}^{N_A}\sum_{j}^{N_B} P(r) \quad (7)$$

where V is the volume, N_A and N_B are the number of atoms (monomers) A and B, respectively, and $P(r)$ is the probability to find a B atom (monomer) at a distance r from an A atom.

III. RESULTS AND DISCUSSION

A. Polymer Melt Simulations. *1. Dimensions of Polymer Chains.* In this section, we will investigate the structure and size of polymer chains in a polymer melt on the basis of predictions from molecular dynamics simulations. Our model differs from that of Kremer and Grest[89] because it contains attraction between the monomers (full Lennard-Jones potential). Also, we use a harmonic potential and not a FENE potential to bond the monomers in the polymer chains.

Hence, in Figure 2, to verify that our model is suitable for ideal polymer melts prior to applying it to nanocomposites, we show as symbols the end-to-end distance $\langle R_e(N)\rangle$ and radius of gyration $\langle R_g(N)\rangle$ of polymers chains of different molecular weights in a polymer melt. In addition, the end-to-end distance and radius of gyration data are fitted with the scaling law $N^{1/2}$ which are shown as solid lines. The fitting is closer to the simulation data for polymer molecular weights greater than the entanglement length N_e, in accordance with the idea that perfect Gaussian statistics are found in the limit $N \rightarrow \infty$. Consequently, the value for the Kuhn length (l_k) of the polymer model for $N = 128$ as calculated from eq 3 ($\langle R_e^2\rangle = l_k L$[86−88]) is $l_k = 1.79\sigma_m$, in agreement within 1% deviation with Kuhn lengths of common polymers (such as atactic polystyrene).[86,87] As can be seen from the inset of Figure 2, $\langle R_e\rangle/\sqrt{6}$ overlaps with $\langle R_g\rangle$ for almost all the polymer molecular weights (for both unentangled and entangled chains), which denotes that the coarse-grained model used in this study can precisely predict ideal polymer chains.[74,87−89]

B. Nanocomposite Simulations. *1. Structural Characterization.* We now focus on the analysis of the static properties of a polymer/SWCNT nanocomposite system. By considering a fixed SWCNT nanotube that spans the simulation cell, we consider an isolated SWCNT nanocomposite with infinite aspect ratio.

We begin by discussing the structural behavior of the polymer chains in a SWCNT nanocomposite system and focusing on the structure in the vicinity of the SWCNT surface for different

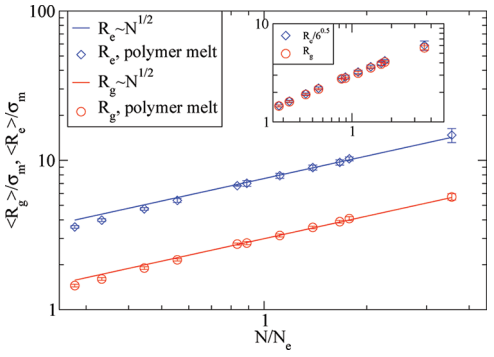

Figure 2. End-to-end distance R_e and radius of gyration R_g of polymer chains of different molecular weight in a monodisperse polymer melt from molecular dynamics simulations: (i) end-to-end distance of a polymer melt (blue diamonds), (ii) fitting of the scaling law $R_e \approx N^{1/2}$ on the simulation data (blue line), (iii) radius of gyration of a polymer melt (red circles), and (iv) fitting of the scaling law $R_g \approx N^{1/2}$ on the simulation data (red line). Inset: R_e normalized with $\sqrt{6}$ and R_g of polymer chains of different molecular weight in a monodisperse polymer melt.

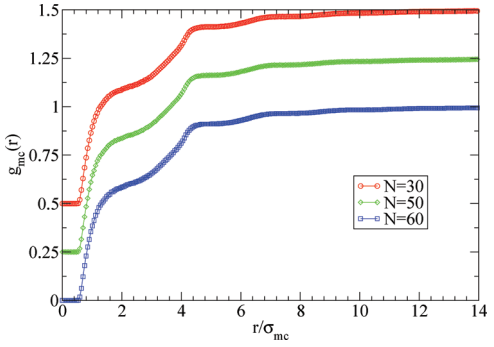

Figure 3. Monomer−carbon radial distribution functions of polymer chains in the polymer/SWCNT ($r_{SWCNT} = 0.66$) nanocomposite system with no interaction with the SWCNT from molecular dynamics simulations: (i) $N = 30$ (red line), (ii) $N = 50$ (green line), and (iii) $N = 60$ (blue line). Data are offset vertically by 0.5 and 0.25 for $N = 30$ and $N = 50$, respectively.

monomer−SWCNT interaction strengths. When there is no interaction between polymer chains and SWCNT, there is only an excluded volume repulsion between the monomers and the carbon atoms of the SWCNT in order to ensure an impenetrable SWCNT. In Figure 3, the monomer−carbon radial distribution function $g_{mc}(r)$ for different polymer molecular weights is depicted. As can be clearly seen, for a very small distance from the SWCNT surface ($r \approx 0.5\sigma_{mc}$), there are no monomers, due to the excluded volume. Subsequently, for $r > 0.5\sigma_{mc}$, there is a layer around the SWCNT where the monomers are depleted due to a reduction of accessible chain conformation in qualitative agreement with theoretical predictions[25−30] and simulation studies[32−35,40,41,46,50,56] of spherical nanoparticles composites. An abrupt almost linear increase is observed from approximately $r > 0.5\sigma_{mc}$ (first monomer next to SWCNT surface) to $r \approx 1.5\sigma_{mc}$ (second monomer from SWCNT surface). Next, a concave regime follows up to $r \approx 2.5\sigma_{mc}$ (second monomer + 1 bond length). Subsequently, a convex regime follows up to a distance $r \approx 4.3\sigma_{mc}$. Finally, the monomer depletion reduces smoothly until the monomer

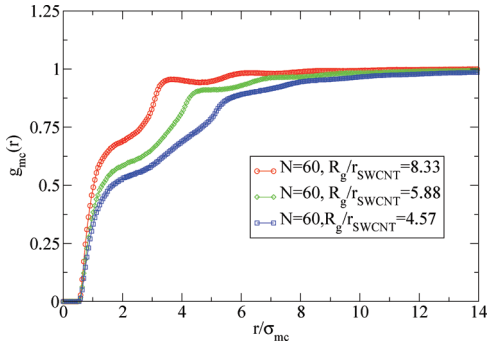

Figure 4. Monomer−carbon radial distribution functions of polymer chains ($N = 60$) in a polymer/SWCNT nanocomposite system with no interaction with the SWCNT from molecular dynamics simulations: (i) $R_g/r_{SWCNT} = 8.33$ (red line), (ii) $R_g/r_{SWCNT} = 5.88$ (green line), and (iii) $R_g/r_{SWCNT} = 4.57$ (blue line).

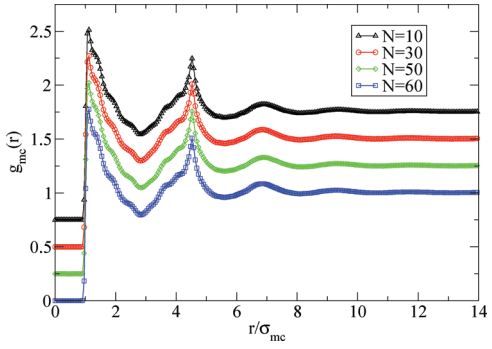

Figure 5. Monomer−carbon radial distribution functions of polymer chains of different molecular weight in a polymer/SWCNT ($r_{SWCNT} = 0.66$) nanocomposite system at kT attractive strength with the SWCNT from molecular dynamics simulations: (i) $N = 10$ (black line), (ii) $N = 30$ (red line), (iii) $N = 50$ (green line), and (iv) $N = 60$ (blue line). Data are offset vertically by 0.75, 0.5, and 0.25 for $N = 10$, $N = 30$, and $N = 50$, respectively.

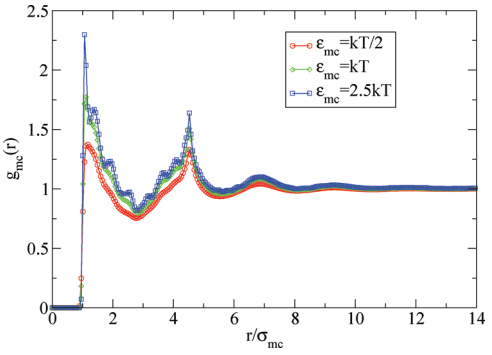

Figure 6. Monomer−carbon radial distribution functions of polymer chains ($N = 60$) in a polymer/SWCNT ($r_{SWCNT} = 0.66$) nanocomposite system at different interaction strengths (ε_{mc}) with the SWCNT from molecular dynamics simulations: (i) $\varepsilon_{mc} = kT/2$ (red line), (ii) $\varepsilon_{mc} = kT$ (green line), and (iii) $\varepsilon_{mc} = 2.5kT$ (blue line).

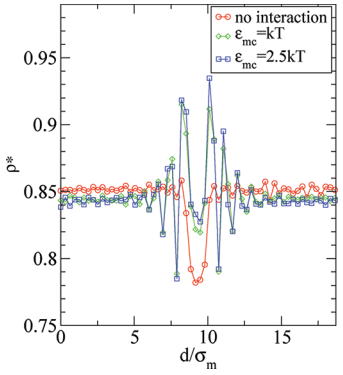

Figure 7. Monomer density vs distance in x direction (perpendicular to the SWCNT) of the simulation cell in a polymer ($N = 60$)/SWCNT ($r_{SWCNT} = 0.66$) nanocomposite system: (i) $\varepsilon_{mc} = 0$ (red symbols), (ii) $\varepsilon_{mc} = kT$ (green symbols), (iii) $\varepsilon_{mc} = 2.5kT$ (blue symbols). The center of SWCNT is located at 9.48.

density reaches its melt value. Moreover, in the case of a constant SWCNT radius, the increase of the size of the polymer chains does not influence the depletion layer around the SWCNT. The thickness of the depletion layer is increased by increasing the radius of the SWCNT as is depicted in Figure 4, in qualitative agreement with the mean-field[25−27,30] and self-consistent-field theories.[28,29] It is worth noting that the depletion layer is approximately of the order of $4\sigma_m$ and that a decrease in the SWCNT radius causes a more pronounced depletion behavior.

Let us now focus on the case where there is an attractive interaction, modeled by the Lennard-Jones potential (eq 1), between polymer chains and SWCNT. In Figure 5, we show the monomer−carbon radial distribution function $g_{mc}(r)$ for different polymer molecular weights. There is no depletion layer around the SWCNT. As can be seen from Figure 5, $g_{mc}(r)$ exhibits a three-layer structure, which is almost indistinguishable for different polymer molecular weights,[90] showing that in this regime the relevant length scale is the density dependent correlation length $\xi(\rho)$. The high monomer density of the layers establish a well-defined interface between SWCNT and polymer melt whose structure differs from that of the amorphous polymer melt. Monomer packing effects become important as monomers form layers around the nanoparticle, which is illustrated by the oscillations of $g_{mc}(r)$.

In Figure 6, the $g_{mc}(r)$ is depicted for polymer chains ($N = 60$) at different interaction strengths between monomers and carbon atoms of the SWCNT. By increasing the interaction of the polymer chains with the SWCNT, the number of contacts with the SWCNT surface increases, so consequently the first peak of the $g_{mc}(r)$ increases accordingly. The effect of increasing the strength of the monomer−carbon attraction alters the density profile at small distances but has little effect on the density at larger distances. In essence, this increase of the attraction leads to a more pronounced layering of monomers around the SWCNT and a greater degree of ordering of the monomers in the radial direction.

To better understand the structural changes in the vicinity of the SWCNT surface, we calculate the monomer density ρ^* as a function of the distance d in the simulation cell. We show $\rho^*(d)$ for the nanocomposite system with (i) nonattractive and (ii) attractive interactions in Figure 7. Only in the second case does the $\rho^*(d)$ show an enhancement in the polymer density near the SWCNT surface in a direction perpendicular to the SWCNT (either x or y) due to the monomer−carbon attraction. The density profile becomes better defined, with larger oscillations, as the interaction strength between monomers and SWCNT surface increases. In the case of nonattractive interactions, depletion of the monomer density in the vicinity of the SWCNT can be seen.

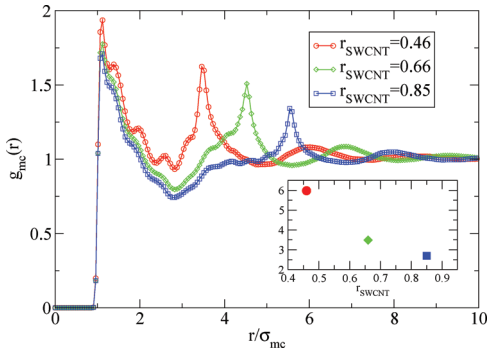

Figure 8. Monomer−carbon radial distribution functions of polymer chains (N = 60) in a polymer/SWCNT nanocomposite system at kT attractive strength for different radius of SWCNT from molecular dynamics simulations: (i) r_{SWCNT} = 0.46 (red line), (ii) r_{SWCNT} = 0.66 (green line), and (iii) r_{SWCNT} = 0.85 (blue line). Inset: the dependence of the volume of the interfacial region relative to the SWCNT volume, quantified by eq 8, on SWCNT radius.

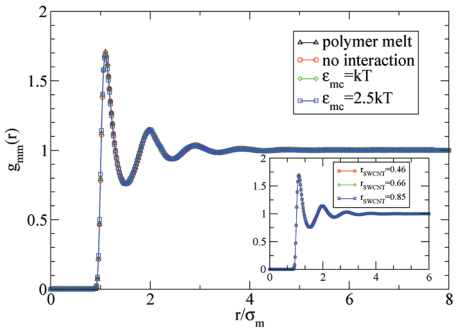

Figure 9. Monomer−monomer radial distribution functions of polymer chains (N = 60) in the polymer/SWCNT (r_{SWCNT} = 0.66) nanocomposite system from molecular dynamics simulations for different interaction strength between monomers and SWCNT surface: (i) ε_{mc} = 0 (red line), (ii) ε_{mc} = kT (green line), and (iii) ε_{mc} = 2.5kT (blue line). Inset: monomer−monomer radial distribution functions of polymer chains (N = 60) in the polymer/SWCNT nanocomposite system from molecular dynamics simulations for ε_{mc} = kT interaction strength between monomers and SWCNT surface for different SWCNT radii: (i) r_{SWCNT} = 0.46 (red line), (ii) r_{SWCNT} = 0.66 (green line), and (iii) r_{SWCNT} = 0.85 (blue line).

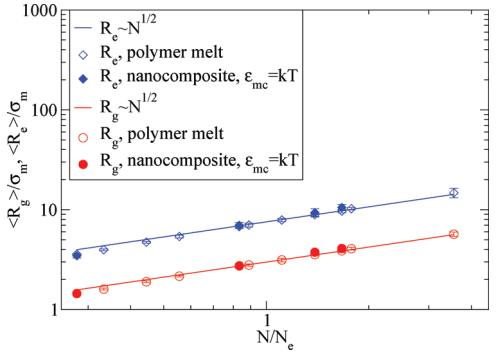

Figure 10. End-to-end distance and radius of gyration of polymer chains of different molecular weight of a polymer/SWCNT (r_{SWCNT} = 0.66) nanocomposite system from molecular dynamics simulations: (i) end-to-end distance of a polymer melt (blue open diamonds), (ii) fitting of the scaling law $R_e \approx N^{1/2}$ on the simulation data (blue line), (iii) end-to-end distance of polymer chains in contact with the SWCNT, interacting with kT energy with the SWCNT (blue filled diamonds), (iv) radius of gyration of a polymer melt (red open circles), (v) fitting of the scaling law $R_g \approx N^{1/2}$ on the simulation data (red line), and (vi) radius of gyration of polymer chains in contact with the SWCNT, interacting with kT energy with the SWCNT (red filled circles).

It is worth mentioning that the presence of a maximum and subsequent oscillation in $\rho^*(d)$ for attractive interactions are also observed in the density profile of monomers near a smooth wall.[49,91−93]

Decreasing the radius of the SWCNT at a constant SWCNT volume fraction increases the surface area of the SWCNT per composite volume. As can been seen from Figure 8, the height of the first peak increases with decreasing radius of the SWCNT, showing that there are more monomer contacts with the SWCNT surface. Closely related to this observation, we also find that a decrease of the SWCNT radius also causes an increase in the peak height of $g_{mc}(r)$ in the second and third layers as the SWCNT radius decreases. The larger peaks with decreasing nanotube radius denote that there is greater molecular ordering in the interface region and lead to a more pronounced layering of monomers. In the inset to Figure 8, we quantify the volume of the interfacial region, relative to the volume of the nanotube using

$$\frac{\int_0^{r_c} g_{mc}(r) r \, dr}{\pi r_{SWCNT}^2} \qquad (8)$$

This quantity decreases as the radius of the nanotube increases, indicating that the interfacial volume, the volume within which the polymer structure is affected by the presence of the nanotubes, relative to the volume of the SWCNT, increases as the radius of the SWCNT decreases. Note that since $g_{mc}(r)$ gradually decays to unity as the radial distance from the nanotube increases, we assume that the cutoff radius for the interfacial region, r_c, and hence the upper limit for the integration to calculate the first moment of $g_{mc}(r)$, is given by the third minimun of $g_{mc}(r)$. However, the same qualitative trend arises if we had chosen, for example, the position of the third maximum for the cutoff.

In Figure 9, we show the total monomer−monomer radial distribution function $g_{mm}(r)$ of polymer chains (N = 60) for both the polymer melt and the polymer/SWCNT nanocomposite systems in the cases of no interaction with the SWCNT and attraction with the SWCNT of the order of kT. There is no alteration of the $g_{mm}(r)$ for all of the cases in the nanocomposite system. Moreover, the $g_{mm}(r)$ for the SWCNT system is indistinguishable from that of the polymer melt system, showing exactly the same structure. Attractive interactions of the order of kT between polymer chains and SWCNT do not influence the monomer structure in the case that the polymer radius of gyration exceeds the radius of the SWCNT. Also, $g_{mm}(r)$ is independent of the SWCNT radius and consequently of the surface area of the SWCNT (see inset of Figure 9).

2. Dimensions of Polymer Chains in Contact with the SWCNT. In Figure 10, we compare $\langle R_e(N)\rangle$ and $\langle R_g(N)\rangle$ of the polymer chains that remain in contact (so polymers in the polymer/SWCNT simulations that do not always contact with SWCNT are ommitted from the value) with the SWCNT with those in the polymer melt. As can be clearly seen, the R_e and R_g of contact polymer chains almost overlap with those in the polymer melt for all the polymer molecular weight when interacting with the SWCNT with kT energy.

dx.doi.org/10.1021/ma201359s |*Macromolecules* 2011, 44, 9830–9838

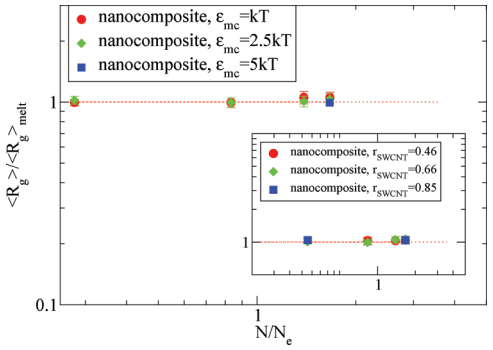

Figure 11. Radius of gyration of polymer chains in contact with the SWCNT of different molecular weight normalized with its bulk value at different interaction strengths between polymer chains and SWCNT (r_{SWCNT} = 0.66) surface: (i) $\varepsilon_{mc} = kT$ (red circles), (ii) $\varepsilon_{mc} = 2.5kT$ (green diamonds), and (iii) $\varepsilon_{mc} = 5kT$ (blue squares). Inset: radius of gyration of polymer chains in contact with the SWCNT of different molecular weight normalized with its bulk value for difference radius of SWCNT at kT interaction strength between polymer chains and SWCNT surface: (i) r_{SWCNT} = 0.46 (red circles), (ii) r_{SWCNT} = 0.66 (green diamonds), and (iii) r_{SWCNT} = 0.85 (blue squares).

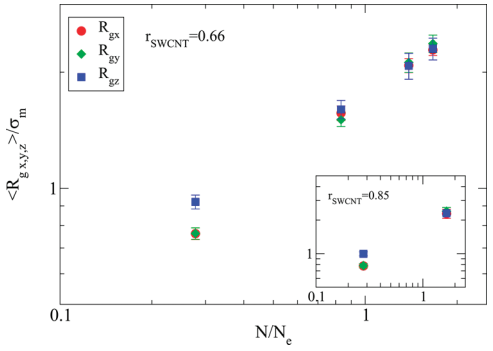

Figure 12. Radius of gyration of polymer chains in contact with the SWCNT (r_{SWCNT} = 0.66) of different molecular weight, interacting with kT energy with the SWCNT, about the x, y, and z axis: (i) $R_{g,x}$ (red circles), (ii) $R_{g,y}$ (green diamonds), (iii) $R_{g,z}$ (blue squares). Inset: radius of gyration of polymer chains in contact with the SWCNT (r_{SWCNT} = 0.85), interacting with kT energy with the SWCNT, about the x, y, and z axis.

In Figure 11, we show the ratio of the radii of gyration of polymer chains which are in contact with the SWCNT to the value in the corresponding pure melt at different interaction strengths between the polymer chains and SWCNT. We observe that R_g of the contact polymer chains retain the melt values for both unentangled and entangled polymer chains, even at very strong levels of attraction between polymer chains and SWCNT ($\varepsilon_{mc} = 5kT$). Similarly, in the inset of Figure 11, we show the same ratio when they interact with kT energy as a function of SWCNT radius. Remarkably, the inset of Figure 11 seems in agreement with Figure 11, where the R_g of the contact polymer chains retain (within 6% deviation) its melt value for both unentangled and entangled polymer chains at any radius of SWCNT smaller than the R_g. In addition, in Figure 12 we show the polymer radius of gyration of polymers in contact with the SWCNT, about the x, y, and z axis ($R_{g,x,y,z}$). We observe that R_g is independent of the different axis except the unentangled polymers (N = 10) where

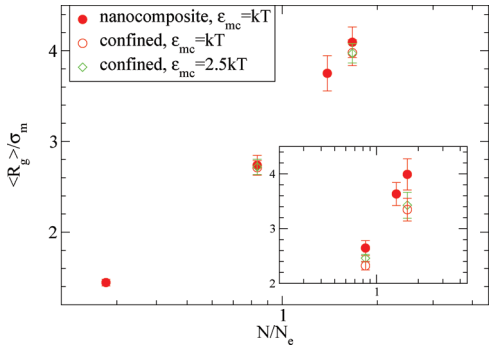

Figure 13. Radius of gyration of polymer chains in contact with the SWCNT (r_{SWCNT} = 0.66) of different molecular weight: (i) one SWCNT, $\varepsilon_{mc} = kT$ (filled circles); (ii) confined system: two SWCNTs, $\varepsilon_{mc} = kT$ (open circles); (iii) confined system: two SWCNTs, $\varepsilon_{mc} = 2.5KT$ (open diamonds). Inset: comparison of radius of gyration of polymer chains in contact with the SWCNT (r_{SWCNT} = 0.66) within R_g distance from the center of the nanotube: (i) one SWCNT, $\varepsilon_{mc} = kT$ (filled circles), (ii) confined system: chains in contact with both SWCNTs, $\varepsilon_{mc} = kT$ (open circles), and (iii) confined system: chains in contact with both SWCNTs, $\varepsilon_{mc} = 2.5kT$ (open diamonds).

in the z direction (parallel to the SWCNT) the short chains "flatten"; thus, R_g appears a larger value in z than the x, y direction. Also, we do not observe any stretching of the polymer chains that are in contact with the nanotube because the polymer radius of gyration is larger than r_{SWCNT}, in contrary to the previous studies[36,39,60] where the nanoparticle radius of curvature is large compared to the R_g, and has an influence on the structure of the polymers in the vicinity of the nanoparticle.

Furthermore, we have performed a few simulations with two SWCNTs present in the simulation cell in order to investigate the role of geometrical confinement on the dimensions of the polymer chains that remain in contact with the carbon nanotube. We observe that the average radius of gyration of the polymer chains that remain in contact with the SWCNT does not change compared to its value in the single SWCNT nanocomposite, as can be seen in Figure 13. However, a few polymer chains which have contacts with both SWCNTs and whose center of mass is within R_g distance from the center of the nanotube reduce the radius of gyration due to the confinement as can be seen in the inset of Figure 13. Because of the small nanotube volume fraction, there are few polymers that are confined in this way. Thus, the overall average radius of gyration is not affected.

Thus, we can conclude that in polymer/SWCNT nanocomposites with radius of SWCNT smaller than the R_g of polymer chains the polymer chains follow unperturbed Gaussian statistics, independent of polymer molecular weight and interaction strength with the SWCNT for an isolated SWCNT. These results are in agreement with a recently studied experimental system of PS with spherical well-dispersed[19,23] or aggregated[21] nanoparticles and with studies for polymer chain dimensions in thin films,[94,95] where it was found that the polymer chains parallel to the surface were unperturbed even for film thickness smaller than R_g.

IV. CONCLUSIONS

In this paper, the structure and conformation of polymer chains in melts and polymer/SWCNT nanocomposite systems were investigated by means of molecular dynamics simulations for both unentangled and entangled polymer chains at isolated

SWCNT. An atomistic model was used for the SWCNT with a large aspect ratio and radius smaller than the polymer chains radius of gyration. Specifically, we find that although the local structure of polymer chains around and nearby the SWCNT is influenced by the interaction strength with the SWCNT, the large scale structure as quantified by the radius of gyration remains unaffected. Although we note that for the shortest chains ($N = 10$) we observe a slight increase in R_g parallel to the SWCNT for chains in contact with the SWCNT. The confinement of the polymer chains by SWCNTs seems to affect only the polymers which have contacts with both of the nanotubes. In particular, in cases where there is no interaction between polymer chains and SWCNT, a depletion layer is presented in the vicinity of SWCNT. When the polymers are attracted to the SWCNT, there is a higher monomer density than its bulk value in the vicinity of the SWCNT. In addition, the monomer density profile of the monomers around the SWCNT surface exhibits pronounced oscillations by increasing the interaction strength with the SWCNT surface. It is worth emphasizing that these results are independent of polymer molecular weight, and interaction strength ($\varepsilon_{mc} = 0kT$ to $\varepsilon_{mc} = 5kT$) with the SWCNT.

AUTHOR INFORMATION

Corresponding Author
*E-mail: n.clarke@sheffield.ac.uk.

ACKNOWLEDGMENT

This research was funded by the EPSRC/NSF Materials Network program EP/5065373/1 (EPSRC: N.C., A.K.) and DMR-0908449 (NSF: K.I.W., R.J.C.).

REFERENCES

(1) Usuki, A.; Kawasumi, M.; Kojima, Y.; Okada, A.; Kurauchi, T.; Kamigaito, O. *J. Mater. Res.* **1993**, *8*, 1174.
(2) Kojima, Y.; Usuki, A.; Kawasumi, M.; Okada, A.; Fukushimay, Y.; Kurauchi, T.; Kamigaito, O. *J. Mater. Res.* **1993**, *8*, 1185.
(3) Moniruzzaman, M.; Winey, K. I. *Macromolecules* **2006**, *39*, 5194.
(4) Winey, K. I.; Vaia, R. A. *MRS Bull.* **2007**, *32*, 314.
(5) Schadler, L. S. *Nature Mater.* **2007**, *6*, 257.
(6) Schadler, L. S.; Brinson, L. C.; Sawyer, W. G. *J. Mater.* **2007**, *59*, 53.
(7) Kumar, S. K.; Krishnamoorti, R. *Annu. Rev. Chem. Biomol. Eng.* **2010**, *1*, 37.
(8) Du, F.; Scogna, R. C.; Zhou, W.; Brand, S.; Fischer, J. E.; Winey, K. I. *Macromolecules* **2004**, *37*, 9048.
(9) Hough, L. A.; Islam, M. F.; Janmey, P. A.; Yodh, A. G. *Phys. Rev. Lett.* **2004**, *93*, 168102.
(10) Winey, K. I.; Kashiwagi, T.; Mu, M. F. *MRS Bull.* **2007**, *32*, 348.
(11) Mu, M.; Clarke, N.; Composto, R. J.; Winey, K. I. *Macromolecules* **2009**, *42*, 7091.
(12) Mu, M.; Composto, R. J.; Clarke, N.; Winey, K. I. *Macromolecules* **2009**, *42*, 8365.
(13) Grady, B. P.; Paul, A.; Peters, J. E.; Ford, W. T. *Macromolecules* **2009**, *42*, 6152.
(14) Simoes, R.; Silva, J.; Vaia, R.; Sencadas, V.; Costa, P.; Gomes, J.; Lanceros-Mendez, S. *Nanotechnology* **2009**, *20*, 035703.
(15) Kim, H.; Abdala, A. A.; Macosko, C. W. *Macromolecules* **2010**, *43*, 6515.
(16) Wong, H. C.; Sanz, A.; Douglas, J. F.; Cabral, J. T. *J. Mol. Liq.* **2010**, *153*, 79.
(17) Karatrantos, A.; Clarke, N. *Soft Matter* **2011**, *7*, 7334.
(18) Nakatani, A. I.; Chen, W.; Schmidt, R. G.; Gordon, G. V.; Han, C. C. *Polymer* **2001**, *42*, 3713.
(19) Mackay, M. E.; Tuteja, A.; Duxbury, P. M.; Hawker, C. J.; Van Horn, B.; Guan, Z.; Chen, G. H.; Krishnan, R. S. *Science* **2006**, *311*, 1740.
(20) Rittigstein, P.; Priestley, R. D.; Broadbelt, L. J.; Torkelson, J. M. *Nature Mater.* **2007**, *6*, 278.
(21) Sen, S.; Xie, Y.; Kumar, S. K.; Yang, H.; Bansal, A.; Ho, D. L.; Hall, L.; Hooper, J. B.; Schweizer, K. S. *Phys. Rev. Lett.* **2007**, *98*, 128302.
(22) Tuteja, A.; Duxbury, P.; Mackay, M. *Phys. Rev. Lett.* **2008**, *100*, 077801.
(23) Jouault, N.; Dalmas, F.; Said, S.; Di Cola, E.; Schweins, R.; Jestin, J.; Boue, F. *Macromolecules* **2010**, *43*, 9881.
(24) Nusser, K.; Neueder, S.; Schneider, G. J.; Meyer, M.; Pyckhout-Hintzen, W.; Willner, L.; Radulescu, A.; Richter, D. *Macromolecules* **2010**, *43*, 9837.
(25) Odijk, T. *Langmuir* **1997**, *13*, 3579.
(26) Odijk, T. *J. Chem. Phys.* **1997**, *106*, 3402.
(27) Fleer, G. J.; Skvortsov, A. M.; Tuinier, R. *Macromolecules* **2003**, *36*, 7857.
(28) Ganesan, V.; Khounlavong, L.; Pryamitsyn, V. *Phys. Rev. E* **2008**, *78*, 051804.
(29) Khounlavong, L.; Ganesan, V. *J. Chem. Phys.* **2009**, *130*, 104901.
(30) Ganesan, V.; Ellison, C. J.; Pryamitsyn, V. *Soft Matter* **2010**, *6*, 4010.
(31) Frischknecht, A. L.; McGarrity, E. S.; Mackay, M. E. *J. Chem. Phys.* **2010**, *132*, 204901.
(32) Kloczkowski, A.; Sharaf, M. A.; Mark, J. E. *Chem. Eng. Sci.* **1994**, *49*, 2889.
(33) Sharaf, M.; Kloczkowski, A.; Mark, J. E. *ACS Polym. Prepr.* **1995**, *36*, 368.
(34) Yuan, Q. W.; Kloczkowski, A.; Sharaf, M. A.; Mark, J. E. *ACS PMSE Prepr.* **1995**, *73*, 374.
(35) Yuan, Q. W.; Kloczkowski, A.; Mark, J. E.; Sharaf, M. A. *J. Polym. Sci., Part B: Polym. Phys.* **1996**, *34*, 1647.
(36) Starr, F. W.; Schroder, T. B.; Glotzer, S. C. *Phys. Rev. E* **2001**, *64*, 021802.
(37) Vacatello, M. *Macromolecules* **2001**, *34*, 1946.
(38) Vacatello, M. *Macromolecules* **2002**, *35*, 8191.
(39) Starr, F. W.; Schroder, T. B.; Glotzer, S. C. *Macromolecules* **2002**, *35*, 4481.
(40) Ozmusul, M. S.; Picu, R. C. *Polymer* **2002**, *43*, 4657.
(41) Smith, G. D.; Bedrov, D.; Li, L.; Byutner, O. *J. Chem. Phys.* **2002**, *117*, 9478.
(42) Smith, J. S.; Bedrov, D.; Smith, G. D. *Compos. Sci. Technol.* **2003**, *63*, 1599.
(43) Bedrov, D.; Smith, G. D.; Smith, J. S. *J. Chem. Phys.* **2003**, *119*, 10438.
(44) Vacatello, M. *Macromol. Theory Simul.* **2003**, *12*, 86.
(45) Vacatello, M. *Macromolecules* **2003**, *36*, 3411.
(46) Doxastakis, M.; Chen, Y.-L.; Guzman, O.; de Pablo, J. J. *J. Chem. Phys.* **2004**, *120*, 9335.
(47) Sharaf, M. A.; Mark, J. E. *Polymer* **2004**, *45*, 3943.
(48) Desai, T.; Keblinski, P.; Kumar, S. K. *J. Chem. Phys.* **2005**, *122*, 134910.
(49) Smith, K. A.; Vladkov, M.; Barrat, J. L. *Macromolecules* **2005**, *38*, 571.
(50) Dionne, P. J.; Osizik, R.; Picu, C. R. *Macromolecules* **2005**, *38*, 9351.
(51) Huang, J.; Mao, Z.; Qian, C. *Polymer* **2006**, *47*, 2928.
(52) Vacatello, M. *Macromol. Theory Simul.* **2006**, *15*, 303.
(53) Zeng, Q. H.; Yu, A. B.; Lu, G. Q. *Prog. Polym. Sci.* **2008**, *33*, 191.
(54) Goswami, M.; Sumpter, B. G. *J. Chem. Phys.* **2009**, *130*, 134910.
(55) Goswami, M.; Sumpter, B. G. *Phys. Rev. E* **2010**, *81*, 041801.
(56) Khounlavong, L.; Pryamitsyn, V.; Ganesan, V. *J. Chem. Phys.* **2010**, *133*, 144904.
(57) Brown, D.; Marcadon, V.; Mele, P.; Alberola, N. D. *Macromolecules* **2008**, *41*, 1499.
(58) Termonia, Y. *Polymer* **2009**, *50*, 1062.
(59) Voyiatzis, G. G.; Voyiatzis, E.; Theodorou, D. N. *Eur. Polym. J.* **2011**, *47*, 699.

(60) Ndoro, T. V. M.; Voyiatzis, E.; Ghanbari, A.; Theodorou, D. N.; Bohm, M. C.; Muller-Plathe, F. *Macromolecules* **2011**, *44*, 2316.
(61) Bansal, A.; Yang, H. C.; Li, C. Z.; Cho, K. W.; Benicewicz, B. C.; Kumar, S. K.; Schadler, L. S. *Nature Mater.* **2005**, *4*, 693.
(62) Sen, S.; Xie, Y.; Bansal, A.; Yang, H.; Cho, K.; Schadler, L. S.; Kumar, S. K. *Eur. Phys. J. Spec. Top.* **2007**, *141*, 161.
(63) Yang, M. J.; Koutsos, V.; Zaiser, M. *J. Phys. Chem. B* **2005**, *109*, 10009.
(64) Wei, C. *Nano Lett.* **2006**, *6*, 1627.
(65) Zheng, Q.; Xue, Q.; Yan, K.; Hao, L.; Li, Q.; Gao, X. *J. Phys. Chem. C* **2007**, *111*, 4628.
(66) Foroutan, M.; Nasrabadi, A. T. *J. Phys. Chem. B* **2010**, *114*, 5320.
(67) Tallury, S. S.; Pasquinelli, M. A. *J. Phys. Chem. B* **2010**, *114*, 4122.
(68) Gurevitch, I.; Srebnik, S. *Chem. Phys. Lett.* **2007**, *444*, 96.
(69) Gurevitch, I.; Srebnik, S. *J. Chem. Phys.* **2008**, *128*, 144901.
(70) Zhao, X. *J. Phys. Chem. C* **2011**, *115*, 6181.
(71) Lu, B.; Maragakis, P.; Kaxiras, E. *Nano Lett.* **2005**, *5*, 897.
(72) Johnson, R. R.; Johnson, A. T. C.; Klein, M. L. *Nano Lett.* **2008**, *8*, 69.
(73) Peter, S.; Meyer, H.; Baschnagel, J. *J. Polym. Sci., Part B: Polym. Phys.* **2006**, *44*, 2951.
(74) Peter, S.; Meyer, H.; Baschnagel, J. *Eur. Phys. J. E* **2009**, *28*, 147.
(75) Allen, M. P.; Tildesley, D. J. *Computer Simulation of Liquids*; Clarendon Press: Oxford, 1987.
(76) Frenkel, D.; Smit, B. *Understanding Molecular Simulation: From Algorithms to Applications (Computational Science)*; Academic Press: New York, 1996.
(77) Bekker, H.; Berendsen, H. J. C.; Dijkstra, E. J.; Achterop, S.; van Drunen, R.; van der Spoel, D.; Sijbers, A.; Keegstra, H.; Reitsma, B.; Renardus, M. K. R. *Phys. Comput.* **1993**, *92*, 252.
(78) Berendsen, H. J. C.; van der Spoel, D.; van Drunen, R. *Comput. Phys. Commun.* **1995**, *91*, 43.
(79) Lindahl, E.; Hess, B.; van der Spoel, D. *J. Mol. Mod.* **2001**, *7*, 306.
(80) van der Spoel, D.; Lindahl, E.; Hess, B.; Groenhof, G.; Mark, A.; Berendsen, H. *J. Comput. Chem.* **2005**, *26*, 1701.
(81) Hoy, R. S.; Foteinopoulou, K.; Kroger, M. *Phys. Rev. E* **2009**, *80*, 031803.
(82) Toepperwein, G. N.; Karayiannis, N. C.; Riggleman, R. A.; Kroger, M.; de Pablo, J. J. *Macromolecules* **2011**, *44*, 1034.
(83) Hoover, W. G. *Phys. Rev. A* **1985**, *31*, 1695.
(84) Nose, S. *Mol. Phys.* **1984**, *52*, 255.
(85) Hockney, R. W.; Goel, S. P.; Eastwood, J. *J. Comput. Phys.* **1974**, *14*, 148.
(86) Flory, P. *Statistical Mechanics of Chain Molecules*; Hanser: Munchen, 1989.
(87) Rubinstein, M.; Colby, R. H. *Polymer Physics*; Oxford University Press: New York, 2003.
(88) Everaers, R.; Sukumaran, S. K.; Grest, G. S.; Svaneborg, C.; Sivasubramanian, A.; Kremer, K. *Science* **2004**, *303*, 823.
(89) Kremer, K.; Grest, G. S. *J. Chem. Phys.* **1990**, *92*, 5057.
(90) Hooper, J. B.; Schweizer, K. S.; Desai, T. G.; Koshy, R.; Keblinski, P. *J. Chem. Phys.* **2004**, *121*, 6986.
(91) Kumar, S. K.; Vacatello, M.; Yoon, D. Y. *J. Chem. Phys.* **1988**, *89*, 5206.
(92) Kumar, S. K.; Vacatello, M.; Yoon, D. Y. *Macromolecules* **1990**, *23*, 2189.
(93) Wang, J. S.; Binder, K. *J. Phys. I* **1991**, *1*, 1583.
(94) Jones, R. L.; Kumar, S. K.; Ho, D. L.; Briber, R. M.; Russell, T. P. *Nature (London)* **1999**, *400*, 146.
(95) Jones, R. L.; Kumar, S. K.; Ho, D. L.; Briber, R. M.; Russell, T. P. *Macromolecules* **2001**, *34*, 559.